Effects of Rotor Bar and End-Ring Faults Over the Signals of a Position Estimation Strategy for Induction Motors

Guillermo R. Bossio, Cristian H. De Angelo, *Member, IEEE*, Guillermo O. García, *Senior Member, IEEE*, Jorge A. Solsona, *Senior Member, IEEE*, and María Inés Valla, *Senior Member, IEEE*

***Abstract*—The effect of rotor faults, such as broken bars and end-rings, over the signals of a position estimation strategy for induction motor drives is analyzed using a multiple coupled circuit model. The objective of this analysis is to establish the possibility of using the estimation strategy signals for fault diagnosis in variable-speed electric drives. This strategy is based on the effect produced by inductance variation on the zero-sequence voltage, when exciting the motor with a predefined inverter switching pattern. Experimental results illustrate the feasibility of the proposal.**

***Index Terms*—Induction motor (IM) drives, position estimation, rotor fault detection.**

I. Introduction

THERE are several proposals designed to detect, online, broken rotor bars on induction motors (IMs). However, there are few of them specifically designed for variable-speed drives. Motor manufacturers are interested in including diagnosis functions in the control software in order to increase their product benefits [1]. For these reasons, fault diagnosis of closed-loop IM drives is an area of further research [2]–[5].

In [3]–[5], the position estimation strategies used in closed-loop IM drives are proposed for fault diagnosis and analysis. These strategies obtain information about the rotor position from the machine saliencies. Such saliencies can be both inherent to the motor manufacture characteristics and created with the purpose of increasing a current or voltage signal that allows the position estimation. The information from the motor saliencies is obtained using an additional excitation to the fundamental one. In some cases, the additional excitation signals are high-frequency three-phase currents or voltages, added to the fundamental excitation [6]. In some others, they are discrete voltage pulses, generated by the inverter, while the fundamental excitation is canceled [7].

The rotor faults modify some IM parameters, such as inductances and resistances, producing saliencies dependent on the rotor position. Consequently, the estimation strategies can be applied for rotor position estimation as well as fault detection and diagnosis. Knowing the fault effects on the position estimation signals leads not only to its detection and analysis but also to the possibility of compensating such effects so as to operate the estimation strategies under nonsevere fault conditions.

To allow analyzing the rotor position estimation and fault diagnosis, an IM model that considers the effects of the different saliencies is needed. The saliencies to be modeled are those that provide information about the rotor position as well as those generated from the fault. In [8], an IM model, based on multiple coupled circuits, and a method known as the "*Winding Function Approach*" (WFA) to calculate mutual inductances, were presented. Regarding the model, all the winding distribution harmonics are taken into account, with no restriction on stator winding and rotor bar symmetry. For such reason, this model can be applied to asymmetric motors and under fault conditions [9]–[12]. A new method to calculate inductances is proposed in [13]. This method is similar to the WFA but it additionally offers modeling the air-gap eccentricity. The authors of this proposal implemented the proposed method to analyze the dynamic eccentricity in a synchronous machine. This method is known as the "*Modified Winding Function Approach*" (MWFA) and it has been applied to analyze IMs with static, dynamic, or mixed eccentricity in [14] and [15]. An extension of this method was proposed in [16]. It allows obtaining inductances, taking into account the radial and axial nonuniformity of both windings and air gap. The application of the multiple coupled circuit model to the analysis of a position estimation strategy, proposed in [7], was presented in [17].

In the previous fault diagnostics proposals based on an additional excitation [3]–[5], strategies based on the injection of high-frequency three-phase signals were mainly analyzed. In this paper, the proposed strategy is based on the effects of winding distribution and rotor bars upon the motor zero-sequence voltage, when the motor is excited with a pre-established discrete pulse sequence applied by the inverter [7]. This strategy offers the advantage of a good signal-to-noise ratio and a low distortion of the fundamental current. The method proposed

Paper IPCSD-05-026, presented at the 2003 IEEE International Electric Machines and Drives Conference, Madison, WI, June 1–4, and approved for publication in the IEEE TRANSACTIONS ON INDUSTRY APPLICATIONS by the Industrial Drives Committee of the IEEE Industry Applications Society. Manuscript submitted for review September 1, 2003 and released for publication March 22, 2005. This work was supported by the Universidad Nacional de Río Cuarto (UNRC), by the Universidad Nacional del Sur (UNS), by the Universidad Nacional de La Plata (UNLP), by ANPCyT, and by CONICET.

G. R. Bossio, C. H. De Angelo, and G. O. García are with the Grupo de Electrónica Aplicada, Facultad de Ingeniería. Universidad Nacional de Río Cuarto, X5804BYA Río Cuarto, Argentina (e-mail: gbossio@ing.unrc.edu.ar; cdeangelo@ieee.org; g.garcia@ieee.org).

J. A. Solsona is with the Departamento de Ingeniería Eléctrica y de Computadoras, Universidad Nacional del Sur, B8000CPB Bahía Blanca, Argentina (e-mail: jsolsona@uns.edu.ar).

M. I. Valla is with the Laboratorio de Electrónica Industrial, Control e Instrumentación, Universidad Nacional de La Plata, 1900 La Plata, Argentina (e-mail: m.i.valla@ieee.org).

Digital Object Identifier 10.1109/TIA.2005.851038

by the authors in [17] is used to analyze the rotor fault effects, such as those from broken bars and end-rings, on the signals generated by the position estimation strategy.

II. IM Model

Considering a motor with m stator circuits and n rotor bars, the rotor cage can be viewed as n-identical, and equally spaced rotor loops plus a loop on one of the end-rings. The voltage equations for the stator and rotor loops can be written in matrix form as

$$\mathbf{V}_s = \mathbf{R}_s \mathbf{I}_s + \frac{d\boldsymbol{\lambda}_s}{dt} \tag{1}$$

$$\mathbf{V}_r = \mathbf{R}_r \mathbf{I}_r + \frac{d\boldsymbol{\lambda}_r}{dt} \tag{2}$$

where $\mathbf{R}_s$ and $\mathbf{R}_r$ are the stator and rotor resistance matrix and

$$\mathbf{V}_s = [\, v_1^s \quad v_2^s \quad \dots \quad v_m^s \,]^T, \tag{3}$$

$$\mathbf{V}_r = [\, 0 \quad 0 \quad \dots \quad 0_n \quad 0_e \,]^T \tag{4}$$

$$\mathbf{I}_s = [\, i_1^s \quad i_2^s \quad \dots \quad i_m^s \,]^T \tag{5}$$

$$\mathbf{I}_r = [\, i_1^r \quad i_2^r \quad \dots \quad i_n^r \quad i_e \,]^T. \tag{6}$$

The fluxes linked by the stator and the rotor are given by

$$\boldsymbol{\lambda}_s = \mathbf{L}_{ss} \mathbf{I}_s + \mathbf{L}_{sr} \mathbf{I}_r, \tag{7}$$

$$\boldsymbol{\lambda}_r = \mathbf{L}_{rs} \mathbf{I}_s + \mathbf{L}_{rr} \mathbf{I}_r. \tag{8}$$

where $\mathbf{L}_{ss}$ is an $m*m$ matrix of the stator mutual inductances, $\mathbf{L}_{rr}$ is an $(n+1)*(n+1)$ matrix of the rotor mutual inductances, $\mathbf{L}_{sr}$ is an $m*(n+1)$ matrix of mutual inductances between the stator phases and the rotor loops, and $\mathbf{L}_{rs}$ is an $(n+1)*m$ matrix of mutual inductances between the rotor loops and the stator phases.

A. Calculation of Inductances

The mutual inductances, used in the multiple coupled circuit model, can be obtained from the equations proposed in [16]. According to this proposal, the mutual inductance between two stator windings and two rotor loops as well as the mutual inductance between a stator winding and a rotor loop, A and B, respectively, can be obtained from

$$L_{BA}(\theta_r) = \mu_0 r \int_0^{2\pi} \int_0^L n_B(\phi, z, \theta_r) N_A(\phi, z, \theta_r) g^{-1}(\phi, z, \theta_r)\, dz\, d\phi \tag{9}$$

where μ_0 is the air permeability, r is the air-gap average radius, L is the stator length, ϕ and z are the angular and axial position of an air-gap arbitrary point, respectively, θ_r is the rotor position, $g^{-1}(\phi, z, \theta_r)$ is the inverse air-gap function, $n(\phi, z, \theta_r)$ is the "*Winding Spatial Distribution*," and $N(\phi, z, \theta_r)$ is the "*Modified Winding Function*." The latter can be obtained as

$$N(\phi, z, \theta_r) = n(\phi, z, \theta_r) - \frac{1}{2\pi L \left\langle g^{-1}(\phi, z, \theta_r) \right\rangle} \times \int_0^{2\pi} \int_0^L n(\phi, z, \theta_r)\; g^{-1}(\phi, z, \theta_r)\, dz\, d\phi \tag{10}$$

where $\left\langle g^{-1}(\phi, z, \theta_r) \right\rangle$ is the average value of the inverse air-gap function.

The distribution of bars and windings by means of winding spatial distribution functions were considered for the calculus of inductances in previous equations. Regarding bar distribution, the skew effects are included, as proposed in [16]. The air-gap variation, due to the rotor slots, was modeled considering the distribution of flux lines on the slots, as proposed in [18].

B. Rotor Fault Modeling

The breakage of a rotor bar or an end-ring can be included in the multiple coupled circuit model by two different ways.

The first one considers that the broken bar is isolated from the rotor core (just like the other bars and the end-rings) and neglects the currents across the rotor core from the broken bar to the others bars and to the end-rings. In such case, the fault can be included in the model as proposed in [9]. For the rotor bar modeling, the breakage of the nth bar is considered. In the proposed model, the equation related to the nth loop is eliminated and the inductances (self and mutual) associated with the $(n-1)$th loop are re-calculated. The breakage of one end-ring is modeled between the first and the nth bar. For this particular case, the equation associated with the nth loop is eliminated and the loop parameters associated with the end-ring are re-calculated. There is an important difference between the effects from rotor bar breakage and those from end-rings. In both cases, the fault produces a modification in a rotor loop. However, in the first case the mutual inductance between the new loop and the stator circuits is larger than in the other loops, while in the second case, the self-inductances in the new loop generated by the breakage of the end-ring are modified. On the other hand, the mutual inductances with the stator circuits do not change.

The second method takes into account that the breakage of a rotor bar or an end-ring produces a significant increase in its resistance, but the current loop is not effectively interrupted, as was previously considered. Then, these faults in the multiple coupled circuits model are included increasing the value of the resistance of either the broken bar or broken end-ring segment.

III. Analysis of Fault Effects on the Position Estimation Signals

The purpose of this work is to analyze the fault effects upon a position estimation strategy, based on the motor inductance variation effects with the rotor position [7]. A scheme of the proposed strategy is shown in Fig. 1. In order to inject the additional excitation signal $\mathbf{V}_{se}^*$, the fundamental current control loop $\mathbf{I}_{sf}^*$ is opened for a short time while the signal $\mathbf{V}_{se}^*$ takes the control of the pulsewidth modulation (PWM) in order to apply the additional excitation signal. This signal consists of the six active inverter states applied in the following sequence: $u_1(+--)$, $u_4(-++)$, $u_3(-+-)$, $u_6(+-+)$, $u_5(--+)$ and $u_2(++-)$ [7].

The zero-sequence voltage is obtained from the sum of the three-phase voltages with respect to the motor neutral point $\mathbf{V}_{sn} = [v_a\ v_b\ v_c]$

$$u_\sigma = v_a + v_b + v_c. \tag{11}$$

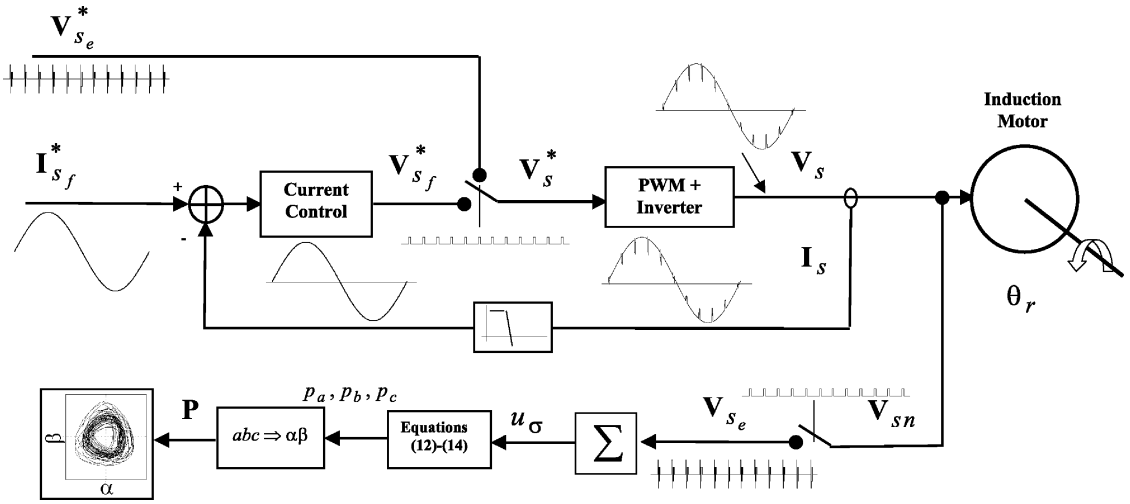

Fig. 1. General scheme of the diagnosis strategy.

These voltages are measured synchronized with the injected voltage pulses.

Subtracting the zero-sequence voltages in the opposite switch positions

$$p_a = u_\sigma^{(1)} - u_\sigma^{(4)} \tag{12}$$

$$p_b = u_\sigma^{(3)} - u_\sigma^{(6)} \tag{13}$$

$$p_c = u_\sigma^{(5)} - u_\sigma^{(2)} \tag{14}$$

where $u_\sigma^{(x)}$ is the zero-sequence voltage corresponding to the u_x inverter state, the speed voltage effects are practically eliminated, and the voltage signal is a function of the excited phase inductances. For an IM with no faults, these three signals are almost sinusoidal and have n periods per revolution, where n is the number of bars.

A spatial vector $\mathbf{P} = (p_\alpha, p_\beta)$, whose angle provides information about the rotor position, can be obtained by transforming the three-phase signals into an α and β coordinate system, fixed to the stator.

The multiple coupled circuit model, previously presented, is used to analyze the effect of the motor inductance on the position estimation signals. If the excitation sequence applied by the inverter corresponds to a small interval of time so that the rotor position and currents remain almost constant, both electromotive force (EMF) and the resistance voltage drops can be neglected in the model. From these practical considerations, the estimation signals p_a, p_b, and p_c are obtained analytically from that model as proposed by the authors in [17]

$$p_a = -2U_d \frac{[1\ 1\ 1]\left(\mathbf{L}_{ss} - \mathbf{L}_{sr}\,\mathbf{L}_{rr}^{-1}\,\mathbf{L}_{rs}\right)^{-1}[2\ -1\ -1]^T}{[1\ 1\ 1]\left(\mathbf{L}_{ss} - \mathbf{L}_{sr}\,\mathbf{L}_{rr}^{-1}\,\mathbf{L}_{rs}\right)^{-1}[1\ 1\ 1]^T} \tag{15}$$

$$p_b = -2U_d \frac{[1\ 1\ 1]\left(\mathbf{L}_{ss} - \mathbf{L}_{sr}\,\mathbf{L}_{rr}^{-1}\,\mathbf{L}_{rs}\right)^{-1}[-1\ 2\ -1]^T}{[1\ 1\ 1]\left(\mathbf{L}_{ss} - \mathbf{L}_{sr}\,\mathbf{L}_{rr}^{-1}\,\mathbf{L}_{rs}\right)^{-1}[1\ 1\ 1]^T} \tag{16}$$

$$p_c = -2U_d \frac{[1\ 1\ 1]\left(\mathbf{L}_{ss} - \mathbf{L}_{sr}\,\mathbf{L}_{rr}^{-1}\,\mathbf{L}_{rs}\right)^{-1}[-1\ -1\ 2]^T}{[1\ 1\ 1]\left(\mathbf{L}_{ss} - \mathbf{L}_{sr}\,\mathbf{L}_{rr}^{-1}\,\mathbf{L}_{rs}\right)^{-1}[1\ 1\ 1]^T} \tag{17}$$

where U_d is the inverter dc-link voltage.

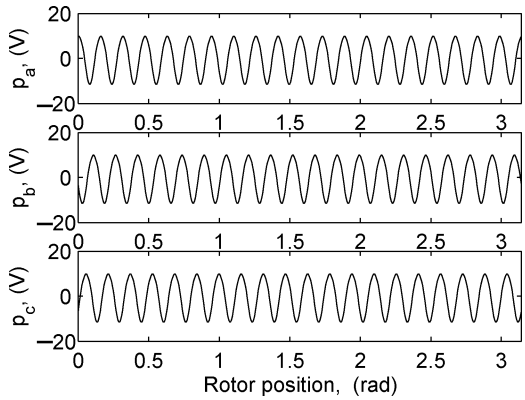

Fig. 2. Analytical result. Signals p_a, p_b, and p_c.

Fig. 2 shows the signals p_a, p_b, and p_c for the motor without faults. These signals were obtained for a three-phase motor whose parameters are shown in the Appendix . These signals show a 40-cycle-per-revolution fundamental frequency due to the inductance variations between the rotor loops and the stator windings. The same signals show a 120° displacement due to the spatial distribution of each phase. For a neater figure, only the results corresponding to half a revolution of the rotor are shown. The signals p_β versus p_α and the p_α signal spectrum are shown in Fig. 3. In the p_α signal spectrum, a 40-cycle-per-revolution component can be clearly observed. There is also an 80-cycle-per-revolution component, which is a function of the motor geometry.

In order to analyze the effects of one or more broken bars, the IM was modeled based on the first proposal presented in the previous section. Fig. 4 shows the signals p_β versus p_α and the p_α signal spectrum for a broken bar. They were analytically calculated from (15)–(17). A zoom of the low-frequency signal spectrum is shown at the top-right corner of Fig. 4. Harmonics of frequency 4 and 8 times higher than that of the rotor mechanical frequency can be observed. These harmonics are due to the interaction of the new bigger rotor loop with each of the four phase poles connected in series. The amplitudes of these harmonics are higher than that of the signals produced by the bars, which does not show amplitude variation at all.

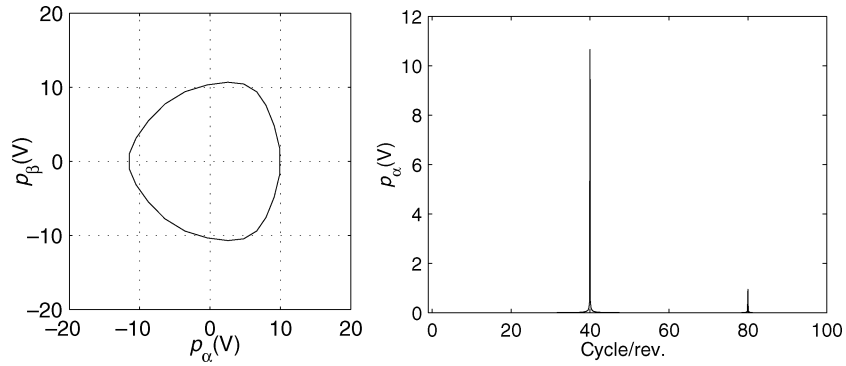

Fig. 3. Analytical result. Signals p_β versus p_α and p_α signal spectrum.

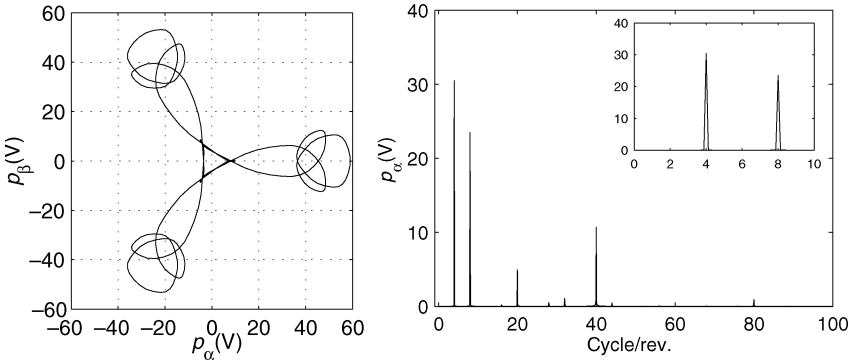

Fig. 4. Analytical result. Signals p_β versus p_α and p_α signal spectrum with a broken bar.

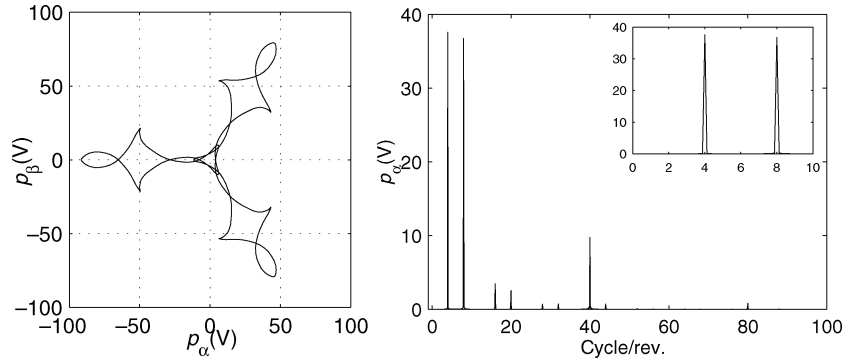

Fig. 5. Analytical result. Signals p_β versus p_α and p_α signal spectrum with a broken end-ring.

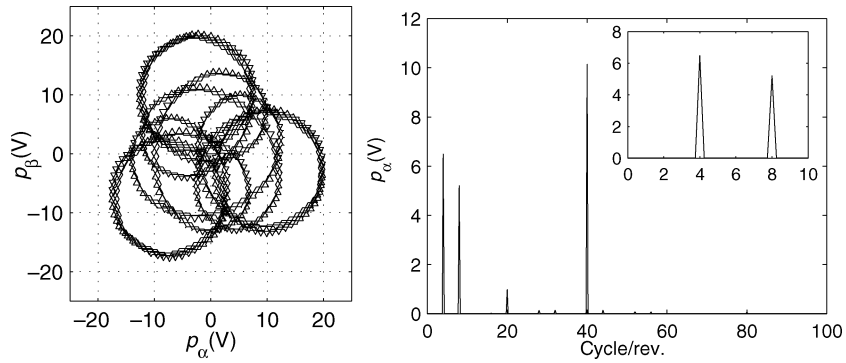

Fig. 6. Simulation result. Signals p_β versus p_α and p_α signal spectrum with a broken bar.

The breakage effects of one of the cage end-rings are shown in p_β versus p_α signals and the p_α signal spectrum (Fig. 5). As in the case of a broken bar, the frequencies 4 and 8 times higher than that of the rotor appears. In this case, the 4- and 8-cycle-per-revolution components show similar amplitude between them, and similar to that of the 4-cycle–per-revolution

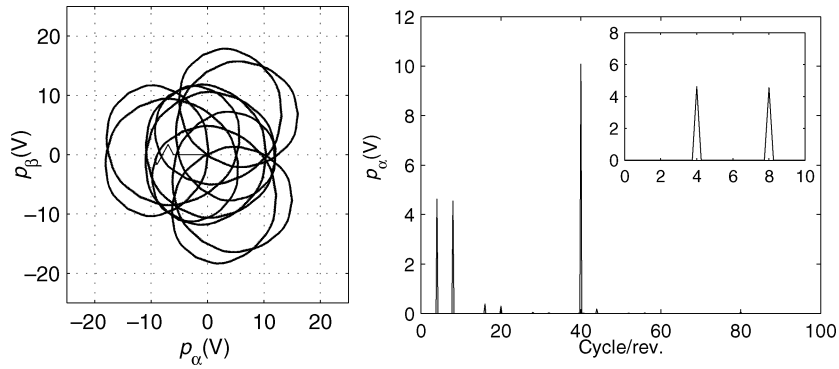

Fig. 7. Simulation result. Signals p_β versus p_α and p_α signal spectrum with a broken end-ring.

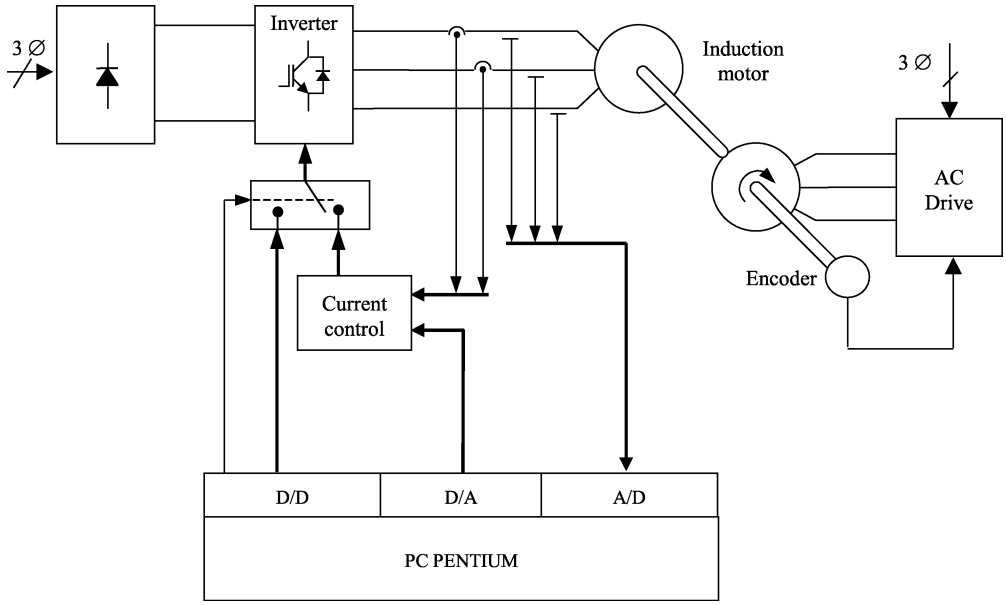

Fig. 8. Experimental setup diagram.

component for one broken bar. In addition, they are almost four times bigger than the signals produced by the bars.

An important difference between the effects produced by the breakages of a rotor bar and an end-ring can be appreciated in the α–β plane, where the path of vector $\mathbf{P}$ appears inverted when the effects of both faults are compared. The cause of this is that, for a broken end-ring, the 4- and 8-cycles-per-revolution components of the p_a, p_b, and p_c signals are in opposite phase. The difference between these two faults can be explained by the fact that the new rotor loop created by the fault has different characteristics for each fault. As described in the previous sections, the new loop originated by a broken bar presents a mutual inductance coupling the stator windings that is greater than those of the remaining rotor loops. Instead, the new loop created by a broken end-ring shows the same mutual inductance, but its self-inductance is greater than those of the other rotor loops.

Since (15)–(17) were obtained neglecting the resistance voltage drops, the diagnosis signals cannot be obtained for the second method proposed in the previous section. For such reason, in order to evaluate the proposed strategy, simulation results were obtained using (1), (2),(7), and (8). The fault

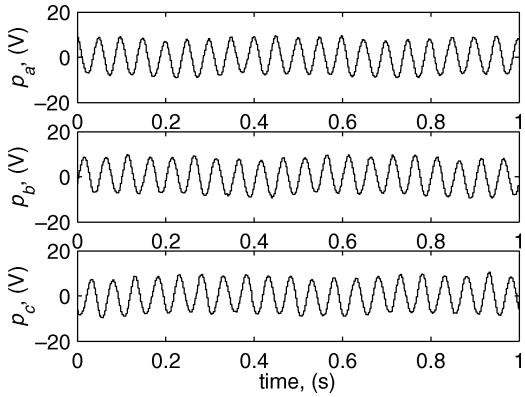

Fig. 9. Experimental result. Signals p_a, p_b, and p_c.

was included by means of an increment in the faulty element resistance. Fig. 6 shows the simulation results for a broken bar. The resistance of the broken bar is 5.5 mΩ, while the resistance of the healthy bars is 32 $\mu\Omega$. Harmonic components equal to those obtained in the analytical way are shown in the simulation results. The amplitude of these components is smaller and it

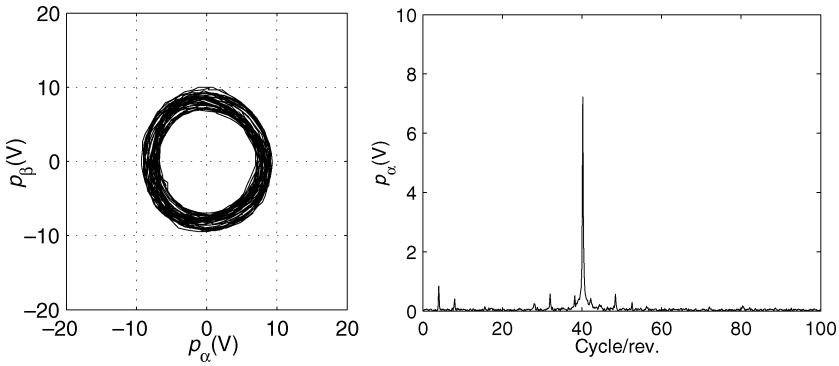

Fig. 10. Experimental result. Signals p_β versus p_α and p_α signal spectrum.

depends on the value of the bar resistance and the frequency of the explorer signal.

Fig. 7 shows the simulation results for the breakage of an end-ring segment, represented by an increment of its resistance from 0.78 $\mu\Omega$ to 2.0 mΩ. Just like in the breakage of a rotor bar, the harmonic components produced by the fault are the same as those obtained by analytical calculation, but their amplitudes are smaller.

IV. Experimental Results

In order to validate the proposed analysis, the estimation strategy was implemented in the laboratory. A diagram of the experimental setup is shown in Fig. 8. The strategy was programmed on a PC with a Pentium processor of 166 Mhz.

The PC has a data acquisition board with A/D and D/A converters and programmable digital inputs/outputs. The fundamental current control loop was performed using delta modulation implemented in an auxiliary board.

The references to the excitation signals, corresponding to a voltage injection of the switching pattern through the inverter, are generated in the PC. The switching between the current control and the excitation signal was implemented in an auxiliary board. The PC, through a digital output of the data acquisition board, carried on the reference for the switching between these two signals.

The software calculates the zero-sequence voltage from measurements of the phase voltages using an A/D input of the acquisition card. The duration of each inverter state associated to a pre-established pulse sequence is 250 μs.

Although in the laboratory the strategy was programmed in a PC, as can be seen in the description of the strategy, it requires a low computational capacity. For this reason, it can be easily implemented in a fixed-point processor of a standard variable-speed drive.

Fig. 9 shows the p_a, p_b, and p_c signals, corresponding to the motor working at 30 r/min, without fundamental excitation and load. The time interval in Fig. 9 corresponds to half a rotor revolution. The signals p_β versus p_α and the p_α signal spectrum are shown in Fig. 10. Figs. 11 and 12 show the same results but with a rotor broken bar (see Fig. 13). The harmonics, obtained experimentally, are the same as those from the model-based analysis. The amplitudes of the 4- and 8-cycle components are very similar to those obtained from simulation and smaller than those

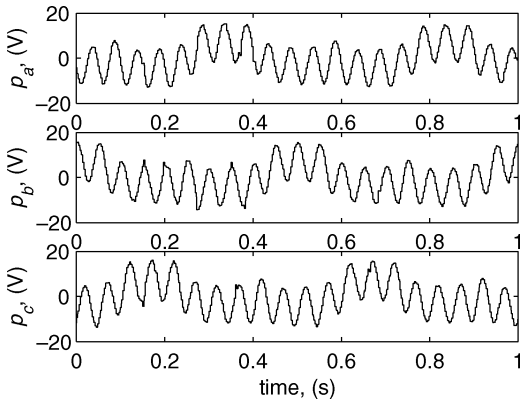

Fig. 11. Experimental result. Signals p_a, p_b, and p_c with a broken bar.

obtained in the analytical form. This is due to the fact that a bar breakage, produced by rotor drilling, yields a significant variation of the bar resistance but not an effective interruption of the rotor loop.

V. Conclusion

In this paper, the rotor fault effects on the signals of a position estimation strategy were analyzed using a multiple coupled circuit model. The modeled rotor faults were broken bars and end-rings. The results showed that such faults produce significant changes in the estimation signals. Consequently, the fault diagnosis and detection from these signals is quite feasible. The experimental results validate the analysis. The inclusion of the fault model in the control algorithm allows position estimation and online fault detection with a moderate increase in the calculation burden.

Appendix
Motor Data

The motor data are as follows:

nominal power: 5.5 kW;
pole pairs: 2;
stator winding: 34 turns per coil, two coils per group, four groups per phase, in-series connection, step 1 :10 : 12;
number of stator slots: 48;
number of rotor bars: 40;
air gap: 0.45 mm;
stator length: 0.11 m;

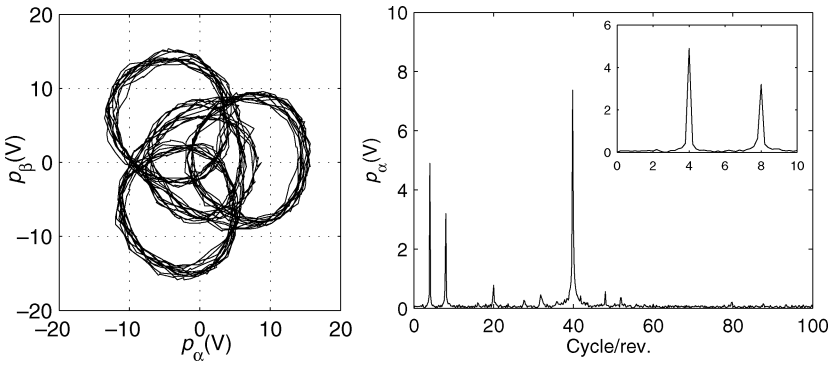

Fig. 12. Experimental result. Signals p_β versus p_α and p_α signal spectrum with a broken bar.

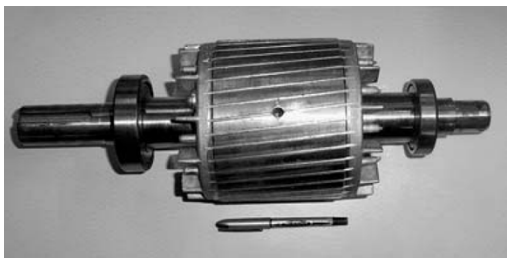

Fig. 13. Rotor with a broken bar.

air-gap average radius: 0.075 m;
skewing: one stator slot period;
rotor slot opening: 2 mm.

REFERENCES

[1] S. Nandi and H. Toliyat, "Condition monitoring and fault diagnosis of electrical machine – A review," in *Conf. Rec. IEEE-IAS Annu. Meeting*, 1999, pp. 197–204.

[2] R. Wieser, C. Kral, F. Pirker, and M. Schagginger, "On-line rotor cage monitoring of inverter-fed induction machines by means of an improved method," *IEEE Trans. Power Electron.*, vol. 14, no. 5, pp. 858–865, Sep. 1999.

[3] A. Bellini, G. Franceschini, N. Petrolini, C. Tassoni, and F. Filippeti, "On-line diagnosis of induction drives rotor by signal injection techniques: Faults location and severity classification," in *Proc. IEE SDEMPED'01*, Grado, Italy, 2001, pp. 531–536.

[4] ——, "Induction machine rotor position detection for diagnostic or control aims: Possibilities and problems," in *Proc. EPE'01*, Graz, Austria, 2001, CD-ROM.

[5] F. Briz, M. W. Degner, A. Zamarrón, and J. M. Guerrero, "On line stator winding fault diagnosis in inverter-fed AC machines using high-frequency signal injection," *IEEE Trans. Ind. Appl.*, vol. 39, no. 4, pp. 1109–1117, Jul./Aug. 2003.

[6] M. Degner and R. Lorenz, "Using multiple saliencies for the estimation of flux, position, and velocity in AC machines," *IEEE Trans. Ind. Appl.*, vol. 34, no. 5, pp. 1097–1104, Sep./Oct. 1998.

[7] J. Jiang and J. Holtz, "Accurate estimation of rotor position and speed of induction motors near standstill," in *Proc. IEEE PEDS'97*, Singapore, 1997, pp. 1–5.

[8] X. Luo, Y. Liao, H. Toliyat, A. El-Antably, and T. A. Lipo, "Multiple coupled circuit modeling of induction machines," *IEEE Trans. Ind. Appl.*, vol. 31, no. 2, pp. 311–318, Mar./Apr. 1995.

[9] H. A. Toliyat and T. A. Lipo, "Transient analysis of cage induction machines under stator, rotor bar and end ring faults," *IEEE Trans. Energy Convers.*, vol. 10, no. 2, pp. 241–247, Jun. 1995.

[10] H. A. Toliyat, M. Areffen, and A. Parlos, "A method for dynamic simulation of air-gap eccentricity in induction machines," *IEEE Trans. Ind. Appl.*, vol. 32, no. 4, pp. 910–918, Jul./Aug. 1996.

[11] M. G. Joksimovic and J. Penman, "The detection of inter-turn short circuits in the stator windings of operating motors," *IEEE Trans. Ind. Electron.*, vol. 47, no. 5, pp. 1078–1084, Oct. 2000.

[12] M. G. Joksimovic, D. M. Durovic, J. Penman, and N. Arthur, "Dynamic simulation of dynamic eccentricity in induction machines-winding function approach," *IEEE Trans. Energy Convers.*, vol. 15, no. 2, pp. 143–148, Jun. 2000.

[13] N. A. Al-Nuaim and H. A. Toliyat, "A novel method for modeling dynamic air-gap eccentricity in synchronous machines based on modified winding function theory," *IEEE Trans. Energy Convers.*, vol. 13, no. 2, pp. 156–162, Jun. 1998.

[14] S. Nandi, R. Bharadwaj, H. Toliyat, and A. Parlos, "Perfomance analysis of a three phase induction motor under mixed eccentricity condition," in *Proc. IEEE PEDES'98*, Perth, Australia, 1998, pp. 123–128.

[15] S. Nandi and H. Toliyat, " Detection of rotor slot and other eccentricity related harmonics in a three phase induction motor with different rotor cages," *IEEE Trans. Energy Convers.*, vol. 16, no. 3, pp. 253–260, Sep. 2001.

[16] G. Bossio, C. De Angelo, J. Solsona, G. García, and M. I. Valla, "A 2D-model of the induction motor: An extension of the modified winding function approach," *IEEE Trans. Energy Convers.*, vol. 19, no. 1, pp. 144–150, Mar. 2004.

[17] G. Bossio, C. De Angelo, J. Solsona, G. García, and M. Valla, "Analysis of a position estimation strategy using a multiple-coupled circuits model of the induction motor," in *Proc. IEEE IECON'02*, 2002, pp. 822–827.

[18] T. Lipo, *Introduction to AC Machine Design*. Madison, WI: Wisconsin Power Electron. Res. Center, Univ. of Wisconsin, 1996, pp. 79–80.

Guillermo R. Bossio received the Electrical Engineer degree from the National University of Río Cuarto, Río Cuarto, Argentina, in 1999, and the Dr. of Engineering degree from the National University of La Plata, La Plata, Argentina, in 2004.

In 1994, he joined the Applied Electronics Group at the National University of Río Cuarto. He is also currently with the National Research Council (CONICET) . His research interests are in electric machines and drives, fault diagnosis of electric machines, and sensorless motor control.

Dr. Bosssio is a Member of the Automatic Control Association of Argentina (AADECA).

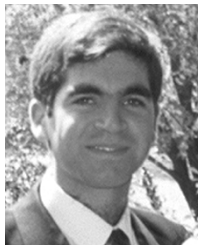

Cristian H. De Angelo (S'96–M'05) received the Electrical Engineer degree from the National University of Río Cuarto, Río Cuarto, Argentina, in 1999, and the Dr. of Engineering degree from the National University of La Plata, La Plata, Argentina, in 2004.

In 1994, he joined the Applied Electronics Group at the National University of Río Cuarto. He is also currently with the National Research Council (CONICET). His research interests are in power electronics, sensorless motor control, electric vehicles, and renewable energy generation.

Dr. De Angelo is a Member of the Automatic Control Association of Argentina (AADECA).

Guillermo O. García (M'86–SM'01) received the Electrical and Electronics Engineering degree from the National University of Córdoba, Córdoba, Argentina, in 1981, and the M.Sc. and Dr. of Electrical Engineering degrees from COPPE, Federal University of Rio de Janeiro, Rio de Janeiro, Brazil, in 1990 and 1994, respectively.

In 1994, he joined the National University of Río Cuarto (UNRC), Río Cuarto, Argentina. Presently, he is Director of the Applied Electronics Group (GEA), Coordinator of a Graduate Program in Electrical Engineering, and a Professor in the Electrical and Electronics Engineering Department, UNRC. He is also currently with the National Research Council (CONICET). His research interests are in power electronics, motion control, electric vehicles, and renewable energy conversion.

Prof. García is a Member of the Automatic Control Association of Argentina (AADECA).

Jorge A. Solsona (S'94–M'96–SM'04) received the Electronics Engineer and Doctor of Engineering degrees from the Universidad Nacional de La Plata, La Plata, Argentina, in 1986 and 1995, respectively.

From 1987 to 1997, he was with the Industrial Electronics, Control and Instrumentation Laboratory, Departamento de Electrotecnia, Facultad de Ingeniería, Universidad Nacional de La Plata. He was with the Departamento de Electrotecnia, Facultad de Ingeniería, Universidad Nacional del Comahue between 1997–2003. Currently, he is with the Instituto de Investigaciones en Ingeniería Eléctrica "Alfredo Desages," Departamento de Ingeniería Eléctrica y Computadoras, Universidad Nacional del Sur, Bahía Blanca, Argentina. He is also currently with the National Research Council (CONICET). He is involved in teaching and research in control theory and its applications to electromechanical systems.

Dr. Solsona is a Member of the Automatic Control Association of Argentina (AADECA).

María Inés Valla (S'79–M'80–SM'97) received the Electronics Engineering and Doctor of Engineering degrees from the National University of La Plata (UNLP), La Plata, Argentina, in 1980 and 1994 respectively.

Currently, she is Full Professor in the Electrical Engineering Department, UNLP. She is also currently with the National Research Council (CONICET). She is engaged in teaching and research in the areas of power converters and ac motor drives.

Dr. Valla is Member of the AdCom of the IEEE Industrial Electronics Society (IES) and is the IES Coordinator of Membership for Region 9. She has been member of the organizing committees of several international conferences. She is also a Member of the Argentina Automatic Control Association (AADECA).